Available online at http://rjas.rsu.ac.th
Formerly Rangsit Journal of Arts and Sciences (RJAS)

Journal of Current Science and Technology, July-December 2020 JCST Vol.10 No.2, pp. 143-153

ISSN 2630-0656 (Online)

Dual-drugs-loaded polymeric nanoparticles formulation design based on response surface methodology of particle size and zeta potential

Benchawan Chamsai[1], Praneet Opanasopit[2] and Wipada Samprasit[1*]

[1]Department of Pharmaceutical Technology, College of Pharmacy, Rangsit University, Patumthani 12000, Thailand.
[2]Department of Pharmaceutical Technology, Faculty of Pharmacy, Silpakorn University, Nakhon Pathom 73000, Thailand.

[*]Corresponding author; E-mail: wipada.s@rsu.ac.th

Received 10 April 2020; Revised 10 July 2020; Accepted 15 July 2020
Published online 20 July 2020

Abstract

Nanoparticles (NPs), particles with at least one dimension below 1000 nm, are frequently used for drug delivery applications. The particle size and zeta potential of NPs can be controlled by the various formulations and processing factors. The purpose of this present study was to optimize dual-drugs (α-mangostin (M) and resveratrol (R))-loaded polymeric NPs. Chitosan (CS) and sodium alginate (ALG) were used to form the NPs via an ionotropic gelation method. A 4-factor, 3-level Box-Behnken Design was conducted for the optimization, choosing the concentrations of CS and ALG and the M and R content as the independent variables. The dependent variables were the particle size and zeta potential of the NPs. The generated polynomial equations and response surface plots were used to relate the dependent and independent variables. The results found that the M and R-loaded CS/ALG NPs were successfully prepared by the ionotropic gelation method, and the CS and ALG had the potential to be used as carriers for the M and R. The ALG concentration affected the particle size of the NPs, while the zeta potential was affected by the CS and ALG concentrations. The M and R content insignificantly affected the particle size and zeta potential of the NPs. The optimized NPs were determined as CS ranging from 0.050 to 0.075 % w/v, ALG ranging from 0.025 to 0.050 % w/v, M ranging from 2.0 to 2.5 % w/w, and R ranging from 1.5 to 2.5 % w/w. Thus, the optimal CS and ALG concentrations and M and R content of the NPs have the potential to be NP carriers for dual-drugs delivery. These NPs might be beneficial for the transdermal and oral delivery of dual-drugs as active antioxidant, antimicrobial and cytotoxic agents.

Keywords**:** *Box-Behnken Design, dual-drugs, nanoparticles, optimization, particle size, zeta potential*

1. Introduction

Nanotechnology for the preparation of nanosized structures containing drug molecules are increasing investigated for drug delivery to diagnose and to treat disease without any side effects (Giri, 2019). Nanoparticles (NPs) are particles with at least one dimension below 1000 nm (Lalatsa, Leite, Figueiredo, & O'Connor, 2018). Usually, NPs with a size ranging between 10-1000 nm are frequently used for drug delivery applications to improve the therapeutic value by protecting drugs from degradation (Kumari, Yadav, & Yadav, 2010) and delivering drugs to the correct location at the appropriate times (De & Robinson, 2003). In addition, these NPs allow reduction of the dosage required, increase drug specificity and bioavailability, overcome chemoresistance, and reduce side effects (Lalatsa et al., 2018). The benefit of NPs for drug delivery systems is controlled by the size of the particles, the surface properties, and the expulsion of therapeutically active agents to achieve the site-specific drug action at a therapeutically optimal rate (Vinothini & Rajan, 2019). Numerous methods available for the preparation of NPs can be classified into two types: top-down methods and bottom-up methods. Top-down techniques make use of mechanical forces with high energy, such as homogenization to reduce the size of the particles to the nanometer range. The bottom-up process of NPs involves the growth of NPs from solution using a magnetic stirrer for mixing, which is a method that can be conducted at relatively low cost with simple equipment (Joseph & Gautam, 2019). Natural and synthetic polymers have been extensively used to prepare nanoparticulate systems (Giri, 2019). Polymeric NPs are widely used for the encapsulation of both hydrophilic and

hydrophobic drugs (Lalatsa et al., 2018). Among the polymers, the biodegradability and nontoxicity of chitosan (CS) and sodium alginate (ALG) make them good candidates for NPs carriers (Elzoghby, Freag, & Elkhodairy, 2018). Furthermore, CS also possesses biocompatibility, homeostasis, and biodegradation that make it a candidate for drug delivery applications (Yadav, Dibi, Mohammed, & Emad, 2019). CS-based NPs can be prepared using an ionotropic gelation method. CS containing amino groups can undergo protonation to produce cationic charge in the acidic pH that is generated by auto-aggregation between CS and macromolecules with an opposite charge, such as ALG (Prabaharan & Mano, 2005). This process is mostly used for the development of CS-based NPs based on their simple, convenient conditions of preparation and the lack of a need for sophisticated equipment. In addition, this operation avoids heat generation, making the processing of thermolabile drugs. Moreover, the uniformity of size problems of CS/ALG NPs needs to be controlled by adjusting the processing parameters.

Various considerable properties that require adequate characterization are included: the particle shape, size, surface area, stability, swelling, agglomeration, and aggregation (Kumar & Dixit, 2017). Particle size is the most basic set of information collected at the beginning of characterization, in which particle size determines the suitability of nanoparticles for drug delivery applications (Kumar & Dixit, 2017). The surface charge of the NPs, termed zeta potential, is another crucial property known to influence the activity of NPs (Nimesh & Gupta, 2017). Moreover, the particle size and zeta potential of NPs play an important role in the transportation and absorption of drugs into the body (Pridgen, Alexis, & Farokhzad, 2014). Thus, the particle size and zeta potential are systematically analyzed in routine research topics (Joseph & Gautam, 2019; Bal, 2019). The size of the NPs can be determined by measuring the random variations in the intensity of the light scattered by a suspension (Bal, 2019), which indicates a NP's diameter (Nanjwadem, Sarkar, & Srichana, 2019). Dynamic light scattering (DLS) is the most common approach to analyze the particle size of NPs (Kumar & Dixit, 2017). The zeta potential is the estimated surface charge, which can be employed for understanding the physical stability of NPs (Joseph & Gautam, 2019; Gaikwad, Choudhari, Bhatia, & Bhatia, 2019) and is a measure of the difference in potential between the bulk fluid in which a NP is dispersed and the layer of fluid containing the oppositely charged ions that is associated with the NP's surface (Selvamani, 2019). The higher the magnitude of potential that is exhibited, the more the electrostatic repulsion and therefore the stability increases (Selvamani, 2019). Basically, the particle size and zeta potential of NPs can be governed by the polymers, which depend on the various formulations and processing factors. The formulation factors include the polymers and the drug concentrations in the reaction mixture (Masalova, Kulikouskaya, Shutava, & Agabekov, 2013). Our previous report stated the optimal CS and ALG ratio (Samprasit, Akkaramongkolporn, Sutananta, & Opanasopit, 2017) and the processing parameters (Samprasit, Akkaramongkolporn, Jaewjira, & Opanasopit, 2018) for the α-mangostin (M)-loaded NPs. However, the dual-drugs-loaded NPs have not been evaluated and reported. M is an active constituent of mangosteen pericarp that was reported to present antioxidant, antibacterial, cytotoxic, anti-inflammatory, and anti-HIV activities (Obolskiy, Pischel, Siriwatanametanon, & Heinrich, 2009). Resveratrol (R) is another natural compound that shows beneficial effects on human health, i.e. slowing the progression of cardiovascular, carcinogenic and neurodegenerative disease, and also has anti-inflammatory, antioxidant and antimicrobial properties. Thus, M and R were chosen for loading into the polymeric NPs. In addition, the formulation factors of dual-drugs-loaded NPs on the particle size and zeta potential have not been systematically reported.

The design of experiments can provide potential support in analyzing the influence of independent variables individually and their interactions with the dependent variables with fewer experimental runs and within minimal time (Niizawa, Espinaco, Zorrilla, & Sihufe, 2019). The response surface methodology is an effective tool for optimizing factors, which is a collection of statistical and mathematical techniques based on the fit of empirical models to the experimental data obtained in relation to the experimental design (Atkinson & Donev, 1992). The Box-Behnken design is the principle design that is commonly used because fewer runs are required in a 4-factor experimental design as compared to central composite design. This design is utilized to

investigate the linears and their interactions on the responses, from which the optimum NPs can be obtained.

2. Objectives

This research was conducted to systematically prepare dual-drugs (M and R)-loaded CS/ALG NPs using an ionotropic gelation method. A combinatorial drug delivery strategy with M and R was carried out in order to study the encapsulation efficiency of the NPs. The 4-factor, 3-level Box-Behnken Design was used to study the effect of the formulation factors on the particle size and zeta potential of the NPs. The formulation factors included the CS and ALG concentrations and the M and R content.

3. Materials and methods

3.1 Materials

M (67%) was extracted from the yellow rubber of mangosteen powder from the pericarp of mangosteen, which was donated by Kaewmungkorn Co., Ltd., Thailand. R (99%), was purchased from Xi'an Gaoyuan Bio-Chem Co., Ltd., China. CS (degree of deacetylation, 0.85; MW, 110 kDa) and the alginic acid sodium salt from brown algae (ALG) were purchased from Sigma, St. Louis, MO, USA. The rest of the reagents were analytical grade. Deionized water was used throughout this entire work.

3.2 Preparation of M and R-loaded NPs

The CS/ALG NPs containing M and R were prepared using an ionotropic gelation method. Briefly, M was dissolved in ethanol and then was slowly added into an aqueous ALG solution. The M and ALG solution was contained in a plastic syringe connected with a 27-gauge, stainless steel needle (diameter, 0.41 mm) at the nozzle and then added dropwise into a CS solution (in 2 % v/v of acetic acid) containing R solution at the solution feeding rate of 1 ml/min. The distance between the steel needle and the CS solution was fixed at 3.5 cm. The mixture was stirred using mechanical stirring at 750 rpm and was further stirred for 30 minutes after the dropping process. The NPs were prepared at 25 °C. The final CS and ALG concentrations were in a range from 0.025 to 0.075 % w/v. The theoretical M and R content was varied at 1, 2 and 3 % w/w of polymer. The final concentration of NPs was dependent upon the concentration of CS and ALG, and M and R content. The pH of the prepared NPs was approximately 5.0 - 5.5. The characteristics of the NPs, including the particle size, size distribution (polydispersity index, PDI) and zeta potential, were observed. The concentration of CS and ALG and the content of M and R in the particles were varied in order to obtain the optimal nanometer particle sizes and zeta potential. The therapeutic range of M and R-loaded NPs are needed for further study. The mean particle size, PDI and zeta potential of the NPs were determined at 25 °C using DLS with a Zetasizer Nano ZS (Malvern Instruments Ltd., Malvern, UK). DLS was used to noninvasively characterize the size of the NPs and accurately measured the particles between 3 nm and 3 μm (Joseph & Gautam, 2019) by measuring the light interference based on the Brownian motion of NPs in suspension (Kumar & Dixit, 2017).

3.3 Optimization employing experimental design

The 4-factor, 3-level Box-Behnken Design was conducted for constructing the polynomial model for the optimization of the M and R-loaded NPs using Minitab Statistical Software version 19 (trial version, Minitab Pty Ltd., Sydney, Australia). Box-Behnken design was selected for the study as it generates fewer runs with four independent variables. The 25 experiments consisting of four independent variables and one replicate at the center point were designed. The independent variables were the concentration of CS and ALG and the M and R content, while the dependent variables selected were the particle size (nm) and zeta potential (mV) of the NPs. The independent and dependent variables are shown in Table 1, and the polynomial equation generated by the experimental design is as follows:

$$Y_i=b_0+b_1X_1+b_2X_2+b_3X_3+b_4X_4+b_{12}X_1X_2+b_{13}X_1X_3+b_{14}X_1X_4+b_{23}X_2X_3+b_{24}X_2X_4+b_{34}X_3X_4+b_{11}X_1^2+b_{22}X_2^2+ b_{33}X_3^2+b_{44}X_4^2 \quad (1)$$

where, Y_i is the response, b_0 is the intercept, and b_i and b_{ij} are the estimated coefficients for the

factors. X_1, X_2, X_3, and X_4 are the coded values of the independent variables. X_aX_b (a, b = 1, 2, 3, 4) represent the interaction and quadratic terms.

The responses are presented in Table 2. The 3D response surface plots were plotted according to the regression model by maintaining one variable at the center level.

Table 1 Independent and dependent variables levels in Box-Behnken design

Independent variables	Coded value Low (–1)	Medium (0)	High (+1)
Independent variables			
X_1 = CS concentration (% w/v)	0.025	0.05	0.075
X_2 = ALG concentration (% w/v)	0.025	0.05	0.075
X_3 = M content (% w/w to polymer)	1	2	3
X_4 = R content (% w/w to polymer)	1	2	3
Dependent variables	**Constraints**		
Y_1 = Particle size of NPs (nm)	Minimize		
Y_2 = Zeta potential of NPs (mV)	Greater than +30 mV or less than –30 mV		

Table 2 The effect of independent variables on the responses of M and R-loaded NPs. Each value represents the mean ± SD from three independent measurements

RUN	Independent variables X_1 (%w/v)	X_2 (% w/v)	X_3 (% w/w)	X_4 (% w/w)	Dependent variables Y_1 (nm)	Y_2 (mV)	PDI
1	0.050	0.050	1	1	948 ± 451	+46.6 ± 1.0	0.498 ± 0.049
2	0.050	0.050	3	1	319 ± 19	+41.6 ± 1.4	1.000 ± 0.000
3	0.050	0.050	1	3	485 ± 179	+43.3 ± 1.1	0.727 ± 0.238
4	0.050	0.050	3	3	390 ± 24	+45.6 ± 1.6	0.672 ± 0.085
5	0.025	0.025	2	2	595 ± 23	+41.1 ± 1.4	0.511 ± 0.088
6	0.075	0.025	2	2	734 ± 122	+52.1 ± 1.1	0.749 ± 0.122
7	0.025	0.075	2	2	2453 ± 1636	–26.4 ± 0.1	0.866 ± 0.232
8	0.075	0.075	2	2	441 ± 3	+40.7 ± 1.1	0.919 ± 0.096
9	0.050	0.025	1	2	656 ± 37	+51.1 ± 0.3	0.484 ± 0.038
10	0.050	0.025	3	2	660 ± 185	+52.4 ± 1.1	0.493 ± 0.029
11	0.050	0.075	1	2	40107 ± 4416	+6.5 ± 0.6	0.332 ± 0.105
12	0.050	0.075	3	2	28990 ± 3652	+25.2 ± 3.6	0.519 ± 0.065
13	0.025	0.050	2	1	643 ± 103	–17.6 ± 0.6	0.565 ± 0.063
14	0.025	0.050	2	3	536 ± 93	–18.8 ± 1.0	0.635 ± 0.072
15	0.075	0.050	2	1	585 ± 83	+55.9 ± 1.2	0.842 ± 0.072
16	0.075	0.050	2	3	2361 ± 1216	+52.0 ± 0.9	0.656 ± 0.032
17	0.025	0.050	1	2	2556 ± 1009	–17.4 ± 0.4	0.839 ± 0.154
18	0.025	0.050	3	2	1294 ± 844	–16.1 ± 0.1	0.592 ± 0.048
19	0.075	0.050	1	2	505 ± 65	+52.8 ± 0.9	0.756 ± 0.044
20	0.075	0.050	3	2	522 ± 121	+51.8 ± 1.1	0.632 ± 0.012
21	0.050	0.025	2	1	668 ± 176	+53.3 ± 0.9	0.530 ± 0.068
22	0.050	0.025	2	3	674 ± 226	+49.9 ± 1.8	0.444 ± 0.029
23	0.050	0.075	2	1	25650 ± 7846	+2.5 ± 0.2	0.558 ± 0.013
24	0.050	0.075	2	3	31773 ± 6698	+8.7 ± 0.5	0.477 ± 0.187
25	0.050	0.050	2	2	503 ± 1	+42.2 ± 0.9	0.752 ± 0.016

4. Results and discussion

The M and R-loaded CS/ALG NPs were successfully prepared by the ionotropic gelation method. The carboxylic groups the stainless steel needle, the distance between the needle solution, the stirring rate and time, the solution feeding rate and temperature, were fixed. All of these fixed parameters ensured that the variation in the NPs characteristics could be due to variations in the CS, ALG, M and R concentrations only.

A total of 25 confirmatory runs were developed by the Box-Behnken design for optimization of the M and R-loaded CS/ALG NPs.

All developed NPs were subjected to characterization, namely, average particle size, PDI and zeta potential. Particle size is the most significant information collected at the beginning of the characterization to determine the suitability of NPs for drug delivery applications (Kumar & Dixit, 2017). PDI presented the distribution of the size populations within a NP formulation. The numerical value of PDI ranged from 0.0 (perfectly uniform NPs) to 1.0 (for highly polydisperse NPs). Zeta potential analysis is routinely employed to monitor the surface charge of NPs in a colloidal

solution (Kumar & Dixit, 2017). This value is used to predict the stability of the NPs in a solution (Kumar & Dixit, 2017). The effect of the independent variables on the dependent variables was investigated and developed (Table 2). Polynomial equations were generated to explain the individual main effects and interaction effects of the independent factors on each of the dependent factors by Minitab Software. The summary of the analysis results for the observed response are shown in Table 3. The effect of each factor was tested using ANOVA with a corresponding P-value. The P-value was less than 0.05, suggesting that the independent variables were significant. The three-dimensional response surface plots and the contour plots for particle size (Y_1) and zeta potential (Y_2) were obtained, as seen in Figures 1 and 2, respectively.

Table 3 The P-value for the independent parameters

Term	P-value	
	Y_1 (nm)	Y_2 (mV)
Constant	0.925	0.000
X_1	0.927	0.000
X_2	0.002	0.000
X_3	0.685	0.655
X_4	0.817	0.967
X_1^2	0.262	0.003
X_2^2	0.021	0.356
X_3^2	0.403	0.783
X_4^2	0.645	0.434
X_1X_2	0.907	0.027
X_1X_3	0.945	0.919
X_1X_4	0.919	0.901
X_2X_3	0.551	0.451
X_2X_4	0.742	0.674
X_3X_4	0.977	0.748

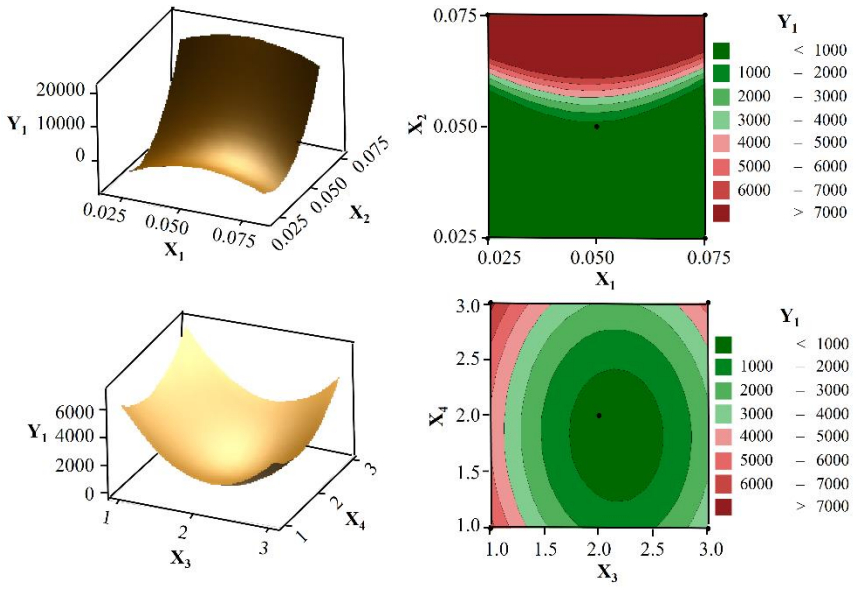

Figure 1 The three-dimensional response surface plots and the contour plots for the effects of variables (X_1: CS concentration, X_2: ALG concentration, X_3: M content and X_4: R content) on the response particle size (Y_1).

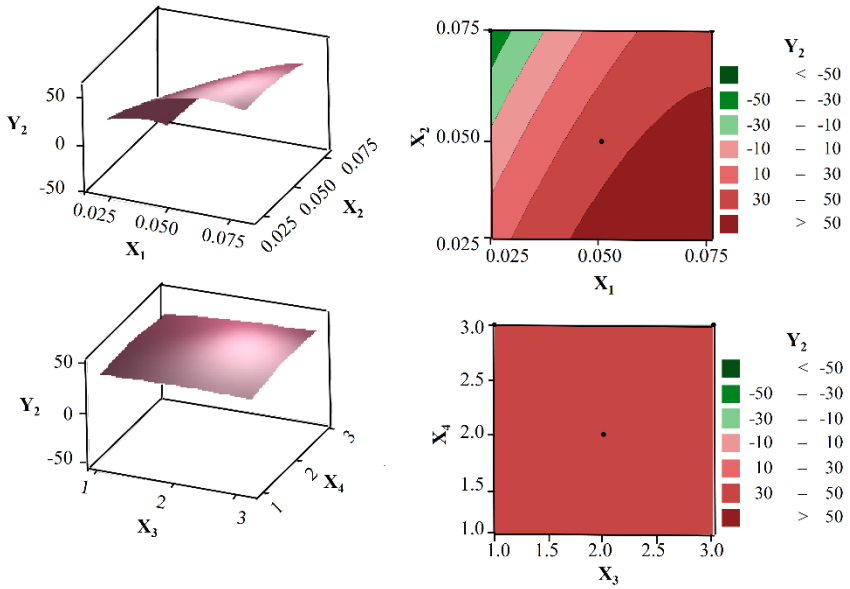

Figure 2 The three-dimensional response surface plots and the contour plots for the effects of variables (X_1: CS concentration, X_2: ALG concentration, X_3: M content and X_4: R content) on the response zeta potential (Y_2).

4.1 Effect of independent variables on particle size and PDI

Particle size is a major factor that influences the interactions of NPs with cells and tissues (Vinothini & Rajan, 2019). In general, NPs with sizes greater than 500 nm enter cells via phagocytosis, whereas smaller NPs are internalized by receptor mediated endocytosis (Vinothini & Rajan, 2019). The NPs were dispersed in an aqueous medium and then characterized by the particle size (Elzoghby et al., 2018). Polymer concentration is known to play an important role in controlling particle size. The particle size of M and R-loaded NPs was found to be in a range from 319 nm (run 2) to 40107·nm (run 11) for different variable combinations (Table 2). As seen in Table 3, it was found that the ALG concentration (X_2) and its interactive influence (X_2^2) were the main factors that affected the particle size. The mathematical model was generated to obtain the final model by the exclusion of non-significant independent variables for particle size (Y_1). The obtained equation explains the influence of the independent variables on the particle size, which was generated as:

$$Y_1 = 16639691X_2^2 - 102530X_2 \quad (2)$$

The mathematical model generated for particle size was found to be significant with F-value of 10.06 ($p = 0.010$) and R^2 value of 0.8061, indicating a good fit. The model explains 80.61 % of the response variability. From the equation, the regression coefficient of the independent variables and their interaction indicated an effect on particle size. The negative coefficients indicated a favorable effect on the particle size (decreased particle size), while the positive coefficients indicated an unfavorable effect on the particle size (increased particle size). The effect on the particle size of the NPs from the ALG concentration was that the increase in the ALG concentration increased the particle size. The probable reason for the increase in the particle size may be that the increase in polymer concentration led to an increase in the viscosity and the formation of particles with larger size at the stirring intensity (750 rpm) (Sharma et al., 2014). The viscosity of 1 % w/v ALG in the aqueous solution was 70 cps. During the preparation of the NPs, the M and ALG solution was injected through a stainless steel needle and then added dropwise into a CS solution. It was more difficult to inject the M and ALG solution when the concentration of ALG increased. In terms of the other factor of X_1, the particle size of NPs seemed to be unchanged when the CS concentration increased from 0.025 to 0.075 % w/v

(Figure 1, upper left and right). The probable reason for this might be explained by the ratio of the CS and ALG. Our previous study reported that the particle size was significantly increased when the ALG concentration was higher than that of the CS (Samprasit et al., 2017). This phenomenon might be attributed to the repulsion between the excess negative charges provided by the ALG molecules in the NPs (Mukhopadhyay, Chakraborty, Bhattacharya, Mishra, & Kundu, 2015). The pH of the prepared NPs (pH~5.0 - 5.5) indicated that CS and ALG had already ionized to positive and negative charges, respectively. According to the contour plots (Figure 1, upper right), CS ranging from 0.025 to 0.075 % w/v and ALG ranging from 0.025 to 0.050 % w/v resulted in the nanometer range of the NPs. Factors X_3 and X_4 (M and R content) showed that the particle size was insignificantly proportional to the amount of M and R (Figure 1, lower left and right). However, the M and R content had a slight effect on the particle size of the NPs. The M and R molecules might have pushed and extended the CS/ALG matrix (Chen, Palazzo, Hennink, & Kok, 2017) and modified the surface of the NPs; thus, the NPs were enlarged (Wang et al., 2018). Only the optimal M (2.0 to 2.5 % w/w) and R (1.5 to 2.5 % w/w) content provided the nanosized particles (Figure 1, lower right). Furthermore, the desirable particle size of NPs for different drug delivery applications was varied. NPs can be administered through an intravenous route in which the enhanced permeability and retention of NPs requires an approximate particle size between 30 and 100 nm (Giri, 2019). Greater than 100-nm-sized NPs were quickly taken up through the reticuloendothelial system. For oral and transdermal delivery, there was not a specified particle size. Particle size affected the interaction of the NPs with tissues and the mechanism of absorption. However, the small size and large surface area of the NPs showed an increase in solubility and thus, the enhanced bioavailability and absorption through the tight junctions of the endothelial cells of the skin (Rizvi & Saleh, 2018). The NPs uptaken by the cells were inversely related to their size (Banerjee et al., 2016). Moreover, CS-based NPs can traverse the mucosal epithelium superior in comparison to microspheres. Due to their small size, they can strongly attach to the mucosa, thus considerably augmenting the residence time in the mucosal tissue (Giri, 2019). NPs may cross the mucosal epithelium intact and can protect drugs from degradation. The PDI of NPs was 0.4 to 1.0, indicating their broad size distribution. Although the processing parameters were controlled, the NPs still had broad size distribution. This might be caused by the manual dropping of the solution.

4.2 Effect of independent variables on zeta potential

The values of zeta potential assessed the stability of the NPs through the strong electrostatic repulsion (Sharma et al., 2014). In general, NPs with zeta potential values greater than +30 mV or less than –30 mV have high degrees of stability (Kumar & Dixit, 2017) and prevent the self-aggregation of NPs (Wu, Zhang, & Watanabe, 2011). In contrast, a small zeta potential value can result in the aggregation and flocculation of NPs due to the van der Waals attractive forces, hydrophobic interactions, and hydrogen bonding (Joseph & Gautam, 2019). The zeta potential of M and R-loaded NPs was found to be in the range of –26.4 mV (run 7) to +55.9·mV (run 15) for different variable combinations (Table 2). As seen in Table 3, it was found that the CS concentration (X_1), ALG concentration (X_2), and the interactive influences of X_1^2 and X_1X_2 were the main factors that affected the zeta potential. The mathematical model was generated to obtain the final model by the exclusion of non-significant independent variables for zeta potential (Y_2), and the obtained equation explains the influence of independent variables on the zeta potential, which was generated as:

$$Y_2 = -6.5 + 3065X_1 - 1731X_2 - 28835X_1^2 + 22467X_1X_2 \quad (3)$$

The mathematical model generated for Y_2 was found to be significant with F-value of 10.69 ($p = 0.000$) and R^2 value of 0.9258, indicating a good fit. The model explains 92.58 % of the response variability. According to the equation, the negative and positive coefficients before the independent variables and their interaction of the quadratic model indicated an effect on the zeta

potential. If the coefficient is positive, the zeta potential will be increased as the variables move from a low to high level; the opposite occurs if the coefficient is negative (Deshmukh & Naik, 2013). A positive value indicates a positive zeta potential while a negative sign presents an inverse effect on the zeta potential (negative value). The positive values were observed by factors X_1 and X_1X_2, while X_2 and X_1^2 had negative values. To compare each independent variable, factor X_1 was more dominant than X_2 with the CS and ALG being positively and negatively charged polymers, respectively. The positive zeta potential increased with the increase of the CS concentration from a low to high level (0.025 to 0.075 % w/v), while the negative zeta potential was found when the ALG concentration increased in the case of lower CS concentration (0.025 to 0.050 % w/v, Figure 2, upper left and right). The interactive influences (X_1^2 and X_1X_2) indicated that the ratio of CS and ALG concentration affected the zeta potential. According to the contour plots (Figure 2, upper right), the negative zeta potential of the NPs was detected when ALG concentration was greater than 0.050 % w/v and 2-fold higher than that of CS. An increase in the ALG concentration resulted in more negative charges neutralizing the positive charge of CS on the surface of the NPs. The CS ranging from 0.050 to 0.075 % w/v and ALG ranging from 0.025 to 0.075 % w/v provided an acceptable range of zeta potential (Figure 2, upper right), except in the case of 0.050 % w/v CS and 0.075 % ALG (runs 11, 12, 23, and 24). This phenomenon might be due to the more dominant positive charge of CS compared with that of the ALG at the acidic pH of the prepared NPs (Rowe, Sheskey, & Owen, 2009). The CS concentration was slightly lower than that of ALG, resulting in the neutralized zeta potential of the NPs. Factors X_3 and X_4, which were the M and R content in the NPs, respectively, showed that the zeta potential was stable when factors X_3 and X_4 were changed (Figure 2, lower left and right). These results also indicated that the insignificant differences in the zeta potentials when M and R were actually loaded into the NPs. Although M and R exist almost entirely in the anion form based on the chemical structure of M and R, the pH condition of the prepared NPs was not suitable for the ionization of M and R. The estimated pK_a of M (3.68, 7.69 and 9.06) and R (8.99, 9.63 and 10.64) indicate that these compounds contain the anion forms when the pH values are higher than the pK_a (National Center for Biotechnology Information, n.d.). Therefore, any of the M and R content (1 to 3 % w/w) could be loaded into the NPs without any changes in the zeta potential (Figure 2, lower right).

To obtain the M and R-loaded NPs, the particle size should be within the nano range and the zeta potential should be optimal. Thus, the concentrations of CS ranging from 0.050 to 0.075 % w/v and ALG ranging from 0.025 to 0.050 % w/v and the loading of M (2.0 to 2.5 % w/w) and R (1.5 to 2.5 % w/w) provided the optimal NPs. Two formulations were randomly selected and testing was performed to ensure this assumption. The particle size and zeta potential of the NPs was determined as shown in Table 4. The selected NPs were in the nanometer range of particle size and an acceptable range of zeta potential, indicating the reliability of the assumption.

Table 4 The particle size and zeta potential of the selected M and R-loaded NPs. Each value represents the mean ± SD

NPs				Particle size (nm)	Zeta potential (mV)
CS (% w/v)	ALG (% w/v)	M (% w/w)	R (% w/w)		
0.050	0.025	2	2	683 ± 163	+ 51.8 ± 1.7
0.075	0.050	2	2	690 ± 47	+ 48.3 ± 0.9

5. Conclusion

CS and ALG have the potential to form the NPs that can be used as carriers for M and R. Box-Behnken design could evaluate the interaction and quadratic effects of the particle size and zeta potential of the NPs. Based on the experimental responses, the ALG concentrations affected the particle size of M and R-loaded NPs, while the zeta potential was affected by the CS and ALG concentrations. The M and R content insignificantly affected the particle size and zeta potential of the NPs. The optimized NPs were determined as CS ranging from 0.050 to 0.075 % w/v, ALG ranging from 0.025 to 0.050 % w/v, M ranging from 2.0 to 2.5 % w/w and R ranging from 1.5 to 2.5 % w/w. Thus, the optimal CS and ALG

concentrations and M and R content of the NPs have the potential to be used as the NP carriers for dual-drugs delivery.

6. Acknowledgements

The authors would like to acknowledge the Commission of Higher Education (Thailand), the Thailand Research Funds through the Research Team Promotion Grant (RTA6180003) for financial supports, College of Pharmacy, Rangsit University for materials and laboratory facilities supports, Ms. Thitiporn Yimpong, Ms. Pichsinee Wongthongkham, and Ms. Tamonwan Prachakitkul for their research assistant.

7. References

Atkinson, A. C., & Donev, A. N. (1992). *Optimum experimental designs.* Oxford, United Kingdom: Oxford University Press.

Bal, Y. (2019). Chapter 11 - Nanomaterials for drug delivery: recent developments in spectroscopic characterization. *Characterization and biology of nanomaterials for drug delivery* (pp. 281-336). DOI: https://doi.org/10.1016/B978-0-12-814031-4.00011-8. Mohapatra, S. S., Ranjan, S., Dasgupta, N., Mishra, R. K., & Thomas, S. Amsterdam, Netherlands: Elsevier.

Banerjee, A., Qi, J., Gogoi, R., Wong, J., & Mitragotri, S. (2016). Role of nanoparticle size, shape and surface chemistry in oral drug delivery. *Journal of Controlled Release, 238*, 176-185. DOI: https://doi.org/10.1016/j.jconrel.2016.07.051

Chen, W., Palazzo, A., Hennink, W. E., & Kok, R. J. (2017). Effect of particle size on drug loading and release kinetics of gefitinib-loaded PLGA microspheres. *Molecular Pharmaceutics, 14*(2), 459-467. DOI: https://doi.org/10.1021/acs.molpharmaceut.6b00896

De, S., & Robinson, D. (2003). Polymer relationships during preparation of chitosan-alginate and poly-l-lysine-alginate nanospheres. *Journal of Controlled Release, 89*(1), 101-112. DOI: https://doi.org/10.1016/S0168-3659(03)00098-1

Deshmukh, R. K., & Naik, B. (2013). Diclofenac sodium-loaded Eudragit® microspheres: Optimization using statistical experimental design. *Journal of Pharmaceutical Innovation, 8*, 276-287. DOI: https://doi.org/10.1007/s12247-013-9167-9

Elzoghby, A. O., Freag, M. S., & Elkhodairy, K. A. (2018). Chapter 7 - Biopolymeric nanoparticles for targeted drug delivery to brain tumors. *Nanotechnology-based targeted drug delivery systems for brain tumors* (pp. 169-190). DOI: https://doi.org/10.1016/B978-0-12-812218-1.00007-5. Kesharwani, P., & Gupta, U. London, United Kingdom: Academic Press.

Gaikwad, V. L., Choudhari, P. B., Bhatia, N. M. & Bhatia, M. S. (2019). Chapter 2 - Characterization of pharmaceutical nanocarriers: in vitro and in vivo studies. *Nanomaterials for drug delivery and therapy* (pp. 32-58). DOI: https://doi.org/10.1016/B978-0-12-816505-8.00016-3. Grumezescu, A. M. Amsterdam, Netherlands: Elsevier.

Giri, T. K. (2019). Chapter 15 - Chitosan based nanoparticulate system for controlled delivery of biological macromolecules. *Nanomaterials for drug delivery and therapy* (pp. 435-459). DOI: https://doi.org/10.1016/B978-0-12-816505-8.00004-7. Grumezescu, A. M. Amsterdam, Netherlands: Elsevier.

Joseph, E. & Gautam, S. (2019). Chapter 4 - Multifunctional nanocrystals for cancer therapy: a potential nanocarrier. *Nanomaterials for drug delivery and therapy* (pp. 91-116). DOI: https://doi.org/10.1016/B978-0-12-816505-8.00007-2. Grumezescu, A. M. Amsterdam, Netherlands: Elsevier.

Kumar, A., & Dixit, C. K. (2017). 3 - Methods for characterization of nanoparticles. *Advances in Nanomedicine for the Delivery of Therapeutic Nucleic Acids* (pp. 43-58). DOI: https://doi.org/10.1016/B978-0-08-100557-6.00003-1. Nimesh, S., Chandra, R., & Gupta, N.Duxford, United Kingdom: Woodhead Publishing.

Kumari, A., Yadav, S. K., & Yadav, S. C. (2010). Biodegradable polymeric nanoparticles based drug delivery systems. *Colloids and Surfaces B: Biointerfaces*, *75*(1), 1-18. DOI: https://doi.org/10.1016/j.colsurfb.2009.09.001

Lalatsa, A., Leite, D. M., Figueiredo, M. F., & O'Connor, M. (2018). Chapter 5 - Nanotechnology in brain tumor targeting: efficacy and safety of nanoenabled carriers undergoing clinical testing. *Nanotechnology-based targeted drug delivery systems for brain tumors* (pp. 111-145). DOI: https://doi.org/10.1016/B978-0-12-812218-1.00005-1. Kesharwani, P., & Gupta, U. London, United Kingdom: Academic Press.

Masalova, O., Kulikouskaya, V., Shutava, T., & Agabekov, V. (2013). Alginate and chitosan gel nanoparticles for efficient protein entrapment. *Physics Procedia*, *40*, 69-75. DOI: https://doi.org/10.1016/j.phpro.2012.12.010

Mukhopadhyay, P., Chakraborty, S., Bhattacharya, S., Mishra, R., & Kundu, P. P. (2015). pH-sensitive chitosan/alginate core-shell nanoparticles for efficient and safe oral insulin delivery. *International Journal of Biological Macromolecules, 72*, 640-648. DOI: https://doi.org/10.1016/j.ijbiomac.2014.08.040

Nanjwadem, B. K., Sarkar, A. B., & Srichana, T. (2019). Chapter 12 - Design and characterization of nanoparticulate drug delivery. *Characterization and biology of nanomaterials for drug delivery* (pp. 337-350). DOI: https://doi.org/10.1016/B978-0-12-814031-4.00012-X. Mohapatra, S.S., Ranjan, S., Dasgupta, N., Mishra, R. K., & Thomas, S. Amsterdam, Netherlands: Elsevier.

National Center for Biotechnology Information. (n.d.). PubChem Database. alpha-Mangostin, CID=5281650. Retrieved May 29, 2020, from https://pubchem.ncbi.nlm.nih.gov/compound/alpha-Mangostin

National Center for Biotechnology Information. (n.d.). PubChem Database. Resveratrol, CID=445154. Retrieved May 29, 2020, from https://pubchem.ncbi.nlm.nih.gov/compound/Resveratrol

Niizawa, I., Espinaco, B. Y., Zorrilla, S. E., & Sihufe, G. A. (2019). Natural astaxanthin encapsulation: Use of response surface methodology for the design of alginate beads. *International Journal of Biological Macromolecules, 121*, 601-608. DOI: https://doi.org/10.1016/j.ijbiomac.2018.10.044

Nimesh, S., & Gupta, N. (2017). 1 - Nanomedicine for delivery of therapeutic molecules. *Advances in Nanomedicine for the Delivery of Therapeutic Nucleic Acids* (pp. 1-12). DOI: https://doi.org/10.1016/B978-0-08-100557-6.00001-8. Nimesh, S., Chandra, R., & Gupta, N. Duxford, United Kingdom: Woodhead Publishing.

Obolskiy, D., Pischel, I., Siriwatanametanon, N., & Heinrich, M. (2009). Garcinia mangostana L.: a phytochemical and pharmacological review. *Phytotheray Research*, *23*(8), 1047-1065. DOI: https://doi.org/10.1002/ptr.2730

Prabaharan, M., & Mano, J. F. (2005). Chitosan-based particles as controlled drug delivery systems. *Drug Delivery*, *12*(1), 41-57. DOI: https://doi.org/10.1080/10717540590889781

Pridgen, E. M., Alexis, F., & Farokhzad, O. C. (2014). Polymeric nanoparticle technologies for oral drug delivery. *Clinical Gastroenterology and Hepatology*, *12*(10), 1605-1610. DOI: https://doi.org/10.1016/j.cgh.2014.06.018

Rizvi, S. A. A., & Saleh, A. M. (2018). Applications of nanoparticle systems in drug delivery technology. *Saudi Pharmaceutical Journal*, *26*(1), 64-70. DOI: https://doi.org/10.1016/j.jsps.2017.10.012

Rowe, R. D., Sheskey, P. J., & Owen, S. C. (2009). *Handbook of Pharmaceutical Excipient*, London: United Kingdom: Pharmaceutical Press.

Samprasit, W., Akkaramongkolporn, P., Jaewjira, S., & Opanasopit, P. (2018). Design of alpha mangostin-loaded chitosan/alginate controlled-release nanoparticles using genipin as crosslinker. *Journal of Drug Delivery Science and Technology*, *46*, 312-321. DOI: https://doi.org/10.1016/j.jddst.2018.05.029

Samprasit, W., Akkaramongkolporn, P., Sutananta, W., & Opanasopit, P. (2017). Effects of chitosan and alginate concentrations on particle size and zeta potential of chitosan- alginate micro/nanoparticles containing α-mangostin. *Bulletin of health science and technology*, *15*(supplement), 72-73. https://www.researchgate.net/publication/342833371

Selvamani, V. (2019). Chapter 15 - Stability Studies on nanomaterials used in drugs. *Characterization and biology of nanomaterials for drug delivery* (pp. 425-444). DOI: https://doi.org/10.1016/B978-0-12-814031-4.00015-5. Mohapatra, S. S., Ranjan, S., Dasgupta, N., Mishra, R. K., & Thomas, S. Amsterdam, Netherlands: Elsevier.

Sharma, D., Maheshwari, D., Philip, G., Rana, R., Bhatia, S., Singh, M., Gabrani, R., Sharma, S. K., Ali, J., Sharma, R. K., & Dang, S. (2014). Formulation and optimization of polymeric nanoparticles for intranasal delivery of lorazepam using Box-Behnken Design: In vitro and in vivo evaluation. *BioMed Research International*, 2014, Article ID 156010. DOI: https://doi.org/10.1155/2014/156010

Vinothini, K., & Rajan, M., (2019). Chapter 9 - Mechanism for the nano-based drug delivery system. *Characterization and biology of nanomaterials for drug delivery* (pp. 219-263). DOI: https://doi.org/10.1016/B978-0-12-814031-4.00009-X. Mohapatra, S.S., Ranjan, S., Dasgupta, N., Mishra, R. K., & Thomas, S. Amsterdam, Netherlands: Elsevier.

Wang, G., Wang, Z., Li, C., Duan, G., Wang, K., Li, Q., & Tao, T. (2018). RGD peptide-modified, paclitaxel prodrug-based, dual-drugs loaded, and redox-sensitive lipid-polymer nanoparticles for the enhanced lung cancer therapy. *Biomedicine & Pharmacotherapy*, *106*, 275-284. DOI: https://doi.org/10.1016/j.biopha.2018.06.137

Wu, L., Zhang, J., & Watanabe, W. (2011). Physical and chemical stability of drug nanoparticles. *Advanced Drug Delivery Reviews*, *63*(6), 456-469. DOI: https://doi.org/10.1016/j.addr.2011.02.001

Yadav, H. K. S., Dibi, M., Mohammed, A., & Emad, A. (2019). Chapter 13 - Thermoresponsive drug delivery systems, characterization, and applications. *Characterization and biology of nanomaterials for drug delivery* (pp. 351-373). DOI: https://doi.org/10.1016/B978-0-12-814031-4.00013-1. Mohapatra, S.S., Ranjan, S., Dasgupta, N., Mishra, R.K., & Thomas, S. Amsterdam, Netherlands: Elsevier.